A New Family of High-Dimensional Molecular Magnets Built from the Manganese−Azido System. Syntheses, Structures, and Magnetic Characterization of Two New Ferro−Antiferromagnetic Two-Dimensional Complexes

Albert Escuer,*,† Ramon Vicente,† Mohamed A. S. Goher,*,‡ and Franz A. Mautner§

Departament de Química Inorgànica, Universitat de Barcelona, Diagonal 647, 08028 Barcelona, Spain, Chemistry Department, Faculty of Science, Kuwait University, P.O. Box 5969 Safat, 13060 Kuwait, and Institut für Physikalische und Theoretische Chemie, Technische Universität Graz, A-8010 Graz, Austria

Received December 12, 1996[⊗]

Two new compounds in the series of general formula $[Mn(L)_2(N_3)_2]_n$ in which L = 4-cyanopyridine (**1**) or 3-acetylpyridine (**2**) have been obtained and structurally and magnetically characterized. Both compounds crystallize in the monoclinic system, space group $P2_1/a$, formula $[C_{12}H_8MnN_{10}]$ with $a = 13.286(4)$ Å, $b = 8.340(3)$ Å, $c = 13.579(4)$ Å, $\beta = 90.55(2)°$, and $Z = 4$ for compound **1** and space group $P2_1/c$, formula $[C_{14}H_{14}MnN_8O_2]$ with $a = 11.843(4)$ Å, $b = 9.550(3)$ Å, $c = 14.998(5)$ Å, $\beta = 105.99(3)°$, and $Z = 4$ for compound **2**. The two compounds show a similar arrangement of alternating end-to-end and end-on azido bridges between the manganese atoms, giving magnetically alternated ferro−antiferromagnetic two-dimensional compounds. The pyridyl ligands coordinated to the axial sites stick out above and below the 2-D sheets, and intersheet $\pi-\pi$ interactions are formed between the pyridyl ligands, playing a role in the structural differences. The low-temperature magnetic properties of **1** and **2**, together with those of the previously reported compounds with L = pyridine (**3**), 4-acetylpyridine (**4**), and ethyl isonicotinate (**5**), are reported. Magnetic ordering and spontaneous magnetization is achieved at $T_C = 18$, 16, 40, 28, and 16 K for **1**−**5**, respectively.

Introduction

The design and characterization of materials exhibiting spontaneous magnetization below a critical temperature (T_C) is one of the current stimulating fields of research for chemists.[1] One approach to the synthesis of materials of this kind consists in the design of high-dimensional compounds obtained from classical molecular chemistry. Several families of molecular-based magnets have been developed in this way in the last few years: Cu(pba) derivatives allow the synthesis of Mn[Cu(pbaOH)]·$2H_2O$ (pba = 1,3-propylenebis(oxamato), $T_C = 30$ K)[2] and $(rad)_2Mn_2[Cu(opba)]_3(DMSO)_2·2H_2O$ (opba = orthophenylenebis(oxamato), rad = nitronyl nitroxide derivative, $T_C = 22.5$ K);[3] oxalato derivatives such as the $(NBu_4)[MCr(oxalate)_3]$ series show T_C in the 6−14 K range depending on M(II).[4] More recently, several Prussian blue analogs show T_C close to room temperature in compounds such as $(Et_4N)_{0.5}Mn_{1.25}[V(CN)_5]·2H_2O$ ($T_C = 230$ K) or the mixed-valence compound $Cr_3[Cr(CN)_6]_2·10H_2O$ ($T_C = 240$ K)[5 a,b] or even at room temperature for the $V[Cr(CN)_6]_{0.86}$ compound ($T_C = 305$ K).[5c] A ferrimagnetically ordered iron−nickel compound has been also reported with $T_C = 8$ K.[6]

In our previous work on the manganese(II)−azido complexes of general formula $[Mn(L)_2(N_3)_2]_n$, where L = pyridine[7,8] (py, **3**), 4-acetylpyridine[9] (4-acpy, **4**), or ethyl isonicotinate[8] (Etinc, **5**), the paramagnetic behavior was studied by relating the structural parameters with the magnitude of the antiferromagnetic coupling for the end-to-end azido bridges.[8] We now present two new complexes of the same general formula in which L = 4-cyanopyridine (4-CNpy) (**1**) or 3-acetylpyridine (3-acpy) (**2**) which show simultaneous end-on and end-to-end azide bridges in an alternating 2-D compound, allowing an unusual ferro−antiferromagnetic arrangement. Here we examine the low-temperature properties of compounds of this type by magnetic susceptibility, magnetization, and EPR measurements. As a result, a new family of molecular-based magnets is presented.

This family of $[Mn(L)_2(N_3)_2]_n$ azido derivatives adds to the growing field of research on the high-dimensional ferro−antiferromagnetic azido systems: Other authors have recently reported the two-dimensional complex $[Ni(2,2\text{-dimethylpropane-1,3-diamine})(N_3)_2]_n$,[10] the 3-D $(NMe_4)[Mn(N_3)_3]_n$,[11] and the two isomeric 2-D and 3-D compounds $[Mn_2(bpym)(N_3)_4]_n$[12,13] (bpym is 2,2′-bipyrimidine). The main purpose of research on these systems is to obtain materials with unusual magnetic properties derived from the ability of the azido group to transmit strong ferro- or antiferromagnetic interactions depending on the coordination mode (end-to-end, antiferromagnetic, end-on fer-

† Universitat de Barcelona (www.ub.es/inorgani/molmag.htm).
‡ Kuwait University.
§ Technische Universität Graz.
⊗ Abstract published in *Advance ACS Abstracts,* July 15, 1997.

(1) Kanh, O. *Molecular Magnetism*; VCH Publishers: New York, 1993.
(2) Kahn, O.; Pei, Y.; Verdaguer, M.; Renard, J. P.; Sletten, J. *J. Am. Chem. Soc.* **1988**, *110*, 782.
(3) Stumpf, H. O.; Ouahab, L.; Pei, Y.; Grandjean, D.; Kahn, O. *Science* **1993**, *261*, 447.
(4) Tamaki, H.; Zhong, Z. J.; Matsumoto, N.; Kida, S.; Koikawa, M.; Achiwa, N.; Hashimoto, Y.; Okawa, H. *J. Am. Chem. Soc.* **1992**, *114*, 6974.
(5) (a) Entley, W. R.; Girolami, G. S. *Science* **1995**, *268*, 397. (b) Mallah, T.; Thiebaut, S.; Verdaguer, M.; Veillet, P. *Science* **1993**, *262*, 1554. (c) Ferlay, S.; Mallah, T.; Ouahès, R.; Veillet, P.; Verdaguer, M. *Nature* **1995**, *378*, 701.
(6) El Fallah, M. S.; Rentschler, E.; Caneschi, A.; Sessoli, R.; Gatteschi, D. *Angew. Chem., Int. Ed. Engl.* **1996**, *35*, 1947.
(7) Goher, M. A. S.; Mautner, F. A. *Croat. Chem. Acta* **1990**, *63*, 559.
(8) Escuer, A.; Vicente, R.; Goher, M. A. S.; Mautner, F. A. *Inorg. Chem.* **1996,** *35*, 6386**.**
(9) Escuer, A.; Vicente, R.; Goher, M. A. S.; Mautner, F. A. *Inorg. Chem.* **1995**, *34*, 5707.
(10) Ribas, J.; Monfort, M.; Solans, X.; Drillon, M. *Inorg. Chem.* **1994**, *33*, 742.
(11) Mautner, F. A.; Cortés, R.; Lezama, L.; Rojo, T. *Angew. Chem., Int. Ed. Engl.* **1995**, *35*, 78.
(12) De Munno, G.; Julve, M.; Viau, G.; Lloret, F.; Faus, J.; Viterbo, D. *Angew. Chem., Int. Ed. Engl.* **1996**, *35*, 1807.
(13) Cortés, R.; Lezama, L.; Pizarro, J. L.; Arriortua, M. I.; Rojo, T. *Angew. Chem., Int. Ed. Engl.* **1996**, *35*, 1810.

S0020-1669(96)01476-0 CCC: $14.00

Table 1. Crystal Data and Structure Refinement for $[Mn(4\text{-}CNpy)_2(N_3)_2]_n$ (**1**) and $[Mn(3\text{-}acpy)_2(N_3)_2]_n$ (**2**)

	1	**2**
chem formula	$C_{12}H_8MnN_{10}$	$C_{14}H_{14}MnN_8O_2$
fw	347.22	381.27
space group	$P2_1/a$	$P2_1/c$
a, Å	13.286(4)	11.843(4)
b, Å	8.340(3)	9.550(3)
c, Å	13.579(4)	14.998(5)
β, deg	90.55(2)	105.99(3)
V, Å^3	1504.6(8)	1630.7(9)
Z	4	4
T, °C	25(2)	25(2)
λ(Mo Kα), Å	0.710 69	0.710 69
ρ_{calc} (ρ_{obs}), g·cm^{-3}	1.533 (1.53(2))	1.553 (1.55(2))
μ(Mo Kα), mm^{-1}	0.893	0.837
R^a	0.0576	0.0785
$R_w{}^{2\,b}$	0.1265	0.2052

[a] $R(F_o) = \sum||F_o| - |F_c||/\sum|F_o|$. [b] $R_w(F_o)^2 = \{\sum[w(F_o)^2 - (F_c)^2)^2]/\sum[w(F_o)^4]\}^{1/2}$.

Table 2. Atomic Coordinates ($\times 10^4$) and Equivalent Isotropic Displacement Parameters (Å^2 $\times$ 10^3) for $[Mn(4\text{-}CNpy)_2(N_3)_2]_n$ (**1**)

	x	y	z	U(eq)[a]
Mn(1)	3963(1)	1204(1)	144(1)	30(1)
N(11)	5566(2)	1358(4)	−317(3)	35(1)
N(12)	5828(3)	2291(4)	−923(3)	37(1)
N(13)	6084(3)	3169(5)	−1522(3)	57(1)
N(21)	2438(3)	654(4)	669(3)	43(1)
N(22)	1855(2)	−307(4)	377(3)	33(1)
N(23)	1248(3)	−1225(4)	110(3)	45(1)
N(1)	3466(2)	750(4)	−1467(3)	37(1)
C(1)	3131(3)	−704(5)	−1752(3)	41(1)
C(2)	2807(3)	−1007(6)	−2696(4)	45(1)
C(3)	2818(3)	208(6)	−3386(3)	44(1)
C(4)	3163(4)	1709(6)	−3104(3)	50(1)
C(5)	3478(4)	1904(6)	−2142(3)	47(1)
C(6)	2507(4)	−66(8)	−4391(4)	66(2)
N(2)	2292(5)	−281(8)	−5201(4)	97(2)
N(3)	4365(2)	1825(4)	1761(3)	36(1)
C(7)	4754(3)	3227(5)	2021(3)	43(1)
C(8)	4987(4)	3640(6)	2985(3)	49(1)
C(9)	4825(4)	2505(6)	3704(3)	45(1)
C(10)	4414(4)	1031(6)	3444(3)	49(1)
C(11)	4194(4)	758(5)	2464(3)	45(1)
C(12)	5072(5)	2790(7)	4734(4)	59(1)
N(4)	5245(4)	2975(7)	5549(4)	85(2)

[a] U(eq) is defined as one-third of the trace of the orthogonalized $\mathbf{U}_{ij}$ tensor.

romagnetic). Order at low temperature has only been found for the former nickel complex (T_C = 55 K) and for the series of compounds reported in this work, due probably to a canting phenomenon.

Experimental Section

Synthesis. Compound **1** was obtained by mixing a solution of $MnCl_2{\cdot}3H_2O$ (4 mmol, 0.79 g) in ethanol (30 mL) with of 4-cyanopyridine (20 mmol, 2.08 g) in ethanol (10 mL). The mixture was heated for several minutes at *ca.* 50 °C followed by dropwise addition of concentrated aqueous solution of sodium azide (10 mmol, 0.65 g). The resulting clear solution was left in a refrigerator for 2 months to growth suitable white crystals of the $[Mn(4\text{-}CNpy)_2(N_3)_2]_n$ complex. Anal. Calcd for $MnC_{12}H_8N_{10}$: C, 41.51; H, 2.32; N, 40.34; Mn, 15.82. Found: C, 41.3; H, 2.2; N, 40.8; Mn, 15.7.

Compound **2** was obtained by the same procedure as **1**, except that the following starting materials were used: $MnCl_2{\cdot}3H_2O$ (3 mmol, 0.59 g), 3-acetylpyridine (8 mmol, 0.97 g), and sodium azide (8 mmol, 0.58 g). The resulting solution was left in a refrigerator in the dark for several weeks to grow well-formed yellow crystals of the $[Mn(3\text{-}acpy)_2(N_3)_2]_n$ complex. Anal. Calcd for $MnC_{14}H_{14}N_8O_2$: C, 44.11; H, 3.70; N, 29.39; Mn, 14.41. Found: C, 44.1; H, 3.6; N, 29.7; Mn, 14.2.

Table 3. Atomic Coordinates ($\times 10^4$) and Equivalent Isotropic Displacement Parameters (Å^2 $\times$ 10^3) for $[Mn(3\text{-}acpy)_2(N_3)_2]_n$ (**2**)

	x	y	z	U(eq)[a]
Mn(1)	4947(1)	30(1)	1173(1)	28(1)
N(11)	5798(4)	1097(5)	192(3)	35(1)
N(12)	6188(5)	2254(6)	282(3)	39(1)
N(13)	6540(7)	3372(7)	362(5)	81(2)
N(21)	5851(5)	1408(6)	2366(4)	44(1)
N(22)	5935(4)	2502(5)	2740(3)	35(1)
N(23)	6042(5)	3597(5)	3123(4)	40(1)
N(1)	6473(4)	−1493(5)	1638(3)	34(1)
C(1)	7545(5)	−1094(6)	2123(4)	36(1)
C(2)	8459(5)	−2008(6)	2476(4)	33(1)
C(3)	8254(6)	−3426(7)	2339(4)	40(1)
C(4)	7147(6)	−3867(7)	1845(5)	45(2)
C(5)	6305(5)	−2880(6)	1515(4)	35(1)
C(6)	9633(5)	−1428(7)	2997(4)	40(1)
C(7)	10711(6)	−2300(9)	3100(5)	53(2)
O(1)	9685(4)	−254(5)	3326(4)	59(1)
N(2)	3418(4)	1596(5)	782(3)	33(1)
C(8)	2358(5)	1180(6)	286(4)	36(1)
C(9)	1397(5)	2077(6)	−43(4)	35(1)
C(10)	1594(5)	3502(7)	157(4)	41(1)
C(11)	2695(6)	3931(6)	657(4)	42(2)
C(12)	3578(5)	2969(6)	948(4)	37(1)
C(13)	247(5)	1517(7)	−594(4)	39(1)
C(14)	−850(6)	2328(8)	−658(5)	53(2)
O(2)	221(5)	400(6)	−984(4)	58(1)

[a] U(eq) is defined as one-third of the trace of the orthogonalized $\mathbf{U}_{ij}$ tensor.

Table 4. Selected Bond Lengths (Å) for $[Mn(4\text{-}CNpy)_2(N_3)_2]_n$ (**1**) and $[Mn(3\text{-}acpy)_2(N_3)_2]_n$ (**2**)

1		**2**	
Manganese Environment			
Mn(1)−N(23B)	2.190(4)	Mn(1)−N(23B)	2.245(5)
Mn(1)−N(21)	2.203(4)	Mn(1)−N(21)	2.241(5)
Mn(1)−N(11)	2.229(3)	Mn(1)−N(11)	2.245(5)
Mn(1)−N(11A)	2.238(3)	Mn(1)−N(11A)	2.266(5)
Mn(1)−N(1)	2.309(4)	Mn(1)−N(1)	2.274(5)
Mn(1)−N(3)	2.313(4)	Mn(1)−N(2)	2.297(5)
Azido Bridges			
N(11)−N(12)	1.187(5)	N(11)−N(12)	1.191(7)
N(12)−N(13)	1.149(5)	N(12)−N(13)	1.140(8)
N(21)−N(22)	1.180(5)	N(21)−N(22)	1.178(7)
N(22)−N(23)	1.168(5)	N(22)−N(23)	1.182(7)

Compounds **3**−**5** were prepared as previously described.[8] Solutions of **1**−**5** at room temperature may be slowly oxidized, but crystalline solids are indefinitely stable.

IR spectra show the characteristic bands attributable to the L ligands (C−N stretching for **1** at 2238 cm^{-1}) and a very strong absorption corresponding to the υ_{as} of the azido groups split into three bands at 2101, 2082, and 2070 cm^{-1} for **1** and 2089, 2057, and 2076 cm^{-1} for **2**.

Spectral and Magnetic Measurements. Infrared spectra (4000−400 cm^{-1}) were recorded from KBr pellets on a Nicolet 520 FTIR spectrophotometer. Magnetic measurements were carried out with a Quantum Design instrument with a SQUID detector, working in the temperature range 300−2 K. The magnetic field was 100 G for the study of the low-temperature phenomena. Magnetization measurements were recorded in the ±5 T range of external magnetic field. Diamagnetic corrections were estimated from the Pascal tables. EPR spectra were recorded at X-band frequency with a Bruker ES200 spectrometer equipped with an Oxford liquid-helium cryostat for variable-temperature work.

Crystallographic Data Collection and Refinement of the Structures. $[Mn(4\text{-}CNpy)_2(N_3)_2]_n$ (1) and $[Mn(3\text{-}acpy)_2(N_3)_2]_n$ (2). The X-ray single-crystal data for both compounds were collected on a modified STOE four-circle diffractometer. Crystal size: 0.55 × 0.30 × 0.22 mm for **1** and 0.65 × 0.30 × 0.22 mm for **2**. The crystallographic data, conditions retained for the intensity data collec-

Table 5. Selected Bond Angles (deg) for $[Mn(4\text{-}CNpy)_2(N_3)_2]_n$ (**1**) and $[Mn(3\text{-}acpy)_2(N_3)_2]_n$ (**2**)

1		**2**	
	Manganese Environment		
N(23B)−Mn(1)−N(21)	98.0(1)	N(23B)−Mn(1)−N(21)	100.3(2)
N(23B)−Mn(1)−N(11)	91.1 (1)	N(23B)−Mn(1)−N(11)	166.4(2)
N(21)−Mn(1)−N(11)	170.8 (1)	N(21)−Mn(1)−N(11)	93.1(2)
N(23B)−Mn(1)−N(11A)	170.6 (1)	N(23B)−Mn(1)−N(11A)	90.7(2)
N(21)−Mn(1)−N(11A)	91.4 (1)	N(21)−Mn(1)−N(11A)	169.0(2)
N(11)−Mn(1)−N(11A)	79.5(1)	N(11)−Mn(1)−N(11A)	75.9(2)
N(23B)−Mn(1)−N(1)	88.6 (1)	N(23B)−Mn(1)−N(1)	86.5(2)
N(21)−Mn(1)−N(1)	91.0(1)	N(21)−Mn(1)−N(1)	88.0(2)
N(11)−Mn(1)−N(1)	90.5 (1)	N(11)−Mn(1)−N(1)	91.7(2)
N(11A)−Mn(1)−N(1)	91.1 (1)	N(11A)−Mn(1)−N(1)	93.0(2)
N(23B)−Mn(1)−N(3)	87.6(1)	N(23B)−Mn(1)−N(2)	92.3(2)
N(21)−Mn(1)−N(3)	86.8(1)	N(21)−Mn(1)−N(2)	89.5(2)
N(11)−Mn(1)−N(3)	92.3 (1)	N(11)−Mn(1)−N(2)	90.1(2)
N(11A)−Mn(1)−N(3)	93.0 (1)	N(11A)−Mn(1)−N(2)	89.7(2)
N(1)−Mn(1)−N(3)	175.3 (1)	N(1)−Mn(1)−N(2)	177.1(2)
Mn(1)−N(11)−Mn(1A)	100.5 (1)	Mn(1)−N(11)−Mn(1A)	104.1(2)
N(12)−N(11)−Mn(1)	121.3(3)	N(12)−N(11)−Mn(1)	125.2(4)
N(12)−N(11)−Mn(1A)	127.9(3)	N(12)−N(11)−Mn(1A)	125.9(4)
N(22)−N(21)−Mn(1)	129.4(3)	N(22)−N(21)−Mn(1)	149.4(4)
N(22)−N(23)−Mn(1B)	141.1(3)	N(22)−N(23)−Mn(1B)	140.1(4)
	Azido Bridges		
N(13)−N(12)−N(11)	178.6(4)	N(13)−N(12)−N(11)	178.7(7)
N(23)−N(22)−N(21)	177.1(4)	N(21)−N(22)−N(23)	178.7(6)

tion, and some features of the structure refinements are listed in Table 1. Graphite-monochromatized Mo Kα radiation ($\lambda = 0.710\ 69$ Å) with the ω-scan technique was used to collect the data sets. The accurate unit-cell parameters were determined from automatic centering of 29 reflections ($8° < \theta < 16°$) for **1** and 40 reflections ($6° < \theta < 12°$) for **2** and refined by least-squares methods. A total of 3697 reflections (2946 independent reflections, R_{int} 0.0548) were collected in the range $2.87° < \theta < 27.50°$ for **1** and 3884 reflections (3170 independent reflections, R_{int} 0.0413) were collected in the range $2.83° < \theta < 27.98°$ for **2**. Two reflections (004; 115) (compound **1**) and ($\bar{3}1\ 0$; $\bar{1}04$) (compound **2**) were collected every 1 h and used for intensity correction (intensity of the two standard reflections dropped continuously during data collection by 22% and 28%, respectively). Corrections were applied for Lorentz−polarization effects, for intensity decay, and for absorption using the DIFABS[14] computer program (range of normalized transmission factors 1.000−0.422 for **1** and 1.000−0.409 for **2**). The structures were solved by direct methods using the SHELXS-86[15] computer program and refined by full-matrix least-squares methods on F^2 (i.e. squared), using the SHELXL-93[16] program incorporated in SHELXTL/PC V 5.03[17] program library and the graphics program PLUTON[18] . All non-hydrogen atoms were refined anisotropically. The hydrogen atoms were located on calculated positions (C−H bond lengths 0.930 Å for aromatic C−H and 0.963 Å for $-CH_3$) and assigned with one (compound **1**) and four (compound **2**) common isotropic displacement factors (separate *U*(iso) for each type of hydrogen in each 3-acpy molecule). The final *R* factors were 0.0576 and 0.0785, respectively, for all observed reflections. The numbers of refined parameters were 209 (**1**) and 232 (**2**). Maximum and minimum peaks in the final difference synthesis were 0.349 and −0.391 e Å^{-3} (**1**) and 1.742 and −0.660 e Å^{-3} (**2**). Final atomic coordinates are reported in Tables 2 and 3, and significant bond parameters for **1** and **2** are given in Tables 4 and 5.

Results and Discussion

Description of the Structures. The labeling diagrams for **1** and **2** are shown in Figures 1 and 2, respectively. The general

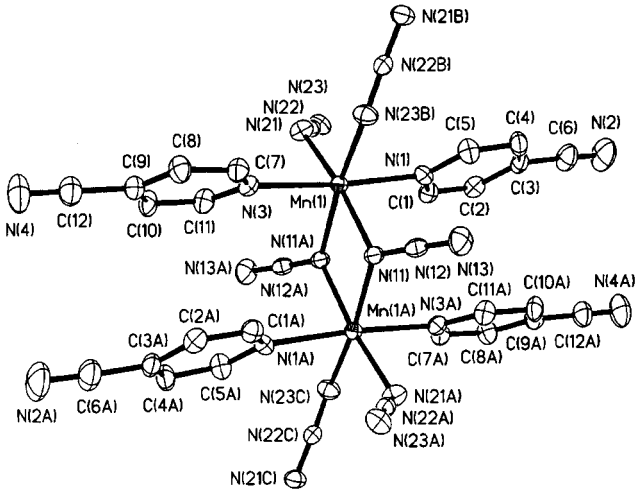

Figure 1. ORTEP drawing (50% of thermal ellipsoid probability) of $[Mn(4\text{-}CNpy)_2(N_3)_2]_n$ (**1**) with atom-labeling scheme.

features of $[Mn(4\text{-}CNpy)_2(N_3)_2]_n$ (**1**) and $[Mn(3\text{-}acpy)_2(N_3)_2]_n$ (**2**) are similar: In both compounds the manganese atoms are coordinated to two nitrogen atoms of the corresponding pyridyl ligand in a *trans* arrangement and the four remaining coordination sites are occupied by four different azido ligands. Two of these azido ligands act as an end-on bridge to a second manganese atom, and the other two act as end-to-end bridges with two new manganese atoms. Then, each manganese atom has three neighboring manganese atoms bridged by azido ligands. This set of bridges, extended as an infinite structure, leads to 2-D compounds in which half of the azido ligands are coordinated in the end-on mode and the other half in the end-to-end mode, Figure 3. The Mn−azido planes of **1** are parallel to the *ab* plane whereas in **2** they are parallel to the *bc* plane. For the two compounds $\pi-\pi$ interactions between the pyridinic rings were found.

$[Mn(4\text{-}CNpy)_2(N_3)_2]_n$ (1). The coordination polyhedron around the manganese atom is slightly elongated along the axis

(14) Walker, N.; Stuart, D. *Acta Crystallogr.* **1983**, *A39*, 158.
(15) Sheldrick, G. M. SHELXS-86, Program for the Solution of Crystal Structure, University of Gottingen, Germany, 1986.
(16) Sheldrick, G. M. SHELXL-93, Program for the Refinement of Crystal Structure, University of Gottingen, Germany, 1993.
(17) SHELXTL 5.03 (PC-Version), Program library for the Solution and Molecular Graphics, Siemens Analytical Instruments Division, Madison, WI, 1995.
(18) Spek, A. L. PLUTON-92, University of Utrecht, 3584, CH Utrecht, The Neederlands, 1992.

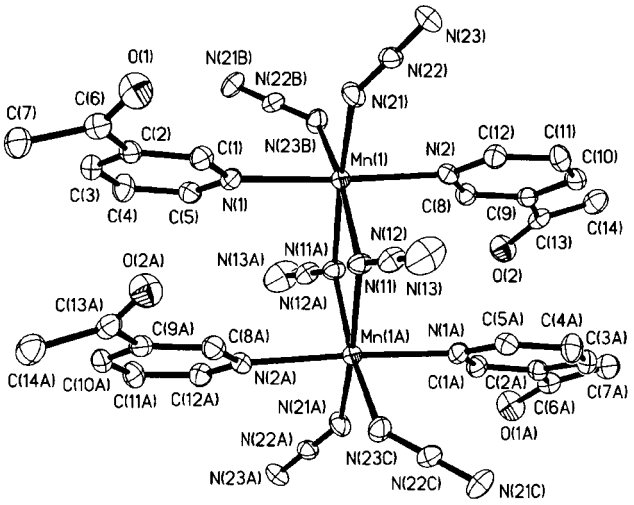

Figure 2. ORTEP drawing (50% of thermal ellipsoid probability) of $[Mn(3\text{-acpy})_2(N_3)_2]_n$ (**2**) with atom-labeling scheme.

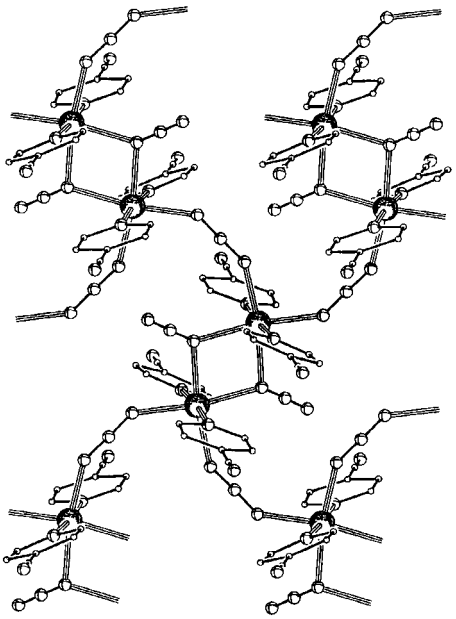

Figure 3. View of a sheet of $[Mn(4\text{-CNpy})_2(N_3)_2]_n$ (**1**) along the *c* axis showing the four end-to-end azido bridges between dimeric $Mn_2(1,1\text{-}\mu\text{-}N_3)_2$ units. The connectivity scheme is the same as for **2**.

defined by the N-pyridyl bonds, Mn(1)−N(1) = 2.309(4) Å and Mn(1)−N(3) = 2.313(4) Å. The four Mn(1)−N(azido) bond distances are close to 2.2 Å. The Mn(1)···Mn(1A) distance is 3.425(2) Å (end-on azido bridges), and the Mn(1)··· Mn(1B) distance is 5.712(2) Å (end-to-end azido bridges). The shortest interplane distances are 13.579(4) Å. The four Mn(1), N(11), Mn(1A), and N(11A) atoms lie strictly on the same plane, and the acute dihedral angle between planes formed by two neighboring Mn_2N_2 units is 20.9(1)°, which gives quasiplanar sheets, Figure 4. The Mn(1)−N(11)−Mn(1A) bond angle of 100.5(1)° lies in the typical range for the end-on azido bridges. The two Mn−N−N bond angles related to the end-to-end bridges are asymmetrical, Mn(1)−N(21)−N(22) = 129.4(3)° and Mn(1B)−N(23)−N(22) = 141.1(3)°. The torsion angle Mn(1)−N(21)···N(23)−Mn(1B) is 58.0(5)°. The pyridyl rings bonded to Mn(1) and Mn(1A), i.e., the axial rings of the end-on units, are tilted 9.8° between them and are separated by around 3.5 Å (Figure 1). This $\pi-\pi$ interaction may contribute to the stability of the end-on units. CN groups of different planes are separated by a similar C−N distance of 3.5 Å.

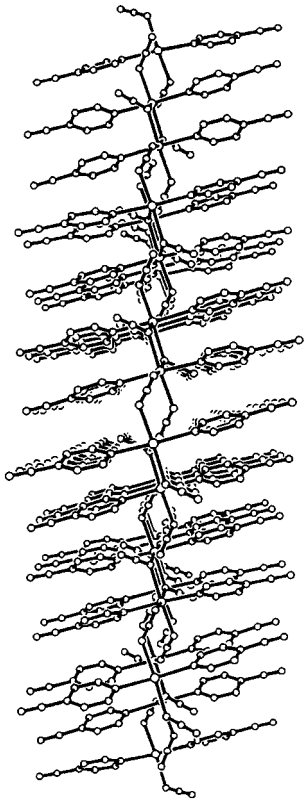

Figure 4. Perspective view of a sheet of $[Mn(4\text{-CNpy})_2(N_3)_2]_n$ (**1**) showing the quasiplanar arrangement of the dimeric $Mn_2(1,1\text{-}\mu\text{-}N_3)_2$ units and the axial arrangement of the *trans* 4-Cnpy ligands that allows the large intersheet separation.

$[Mn(3\text{-acpy})_2(N_3)_2]_n$ (2). The coordination polyhedron around the manganese atom is quite regular with all the bond distances comprised in the range 2.241(5)−2.297(5) Å. The Mn(1)···Mn(1A) distance is 3.556(2) Å, slightly greater than that of compound **1** due to the greater Mn(1)−N(11)−Mn(1A) = 104.1(2)° bond angle (end-on azido bridges), and the Mn(1)···Mn(1B) distance is 6.195(2) Å also due to the greater Mn−N−N bond angles Mn(1)−N(21)−N(22) = 149.4(4)° and Mn(1B)−N(23)−N(22) = 140.1(4)° related to the end-to-end bridges. The Mn···Mn shortest interplane distance is 11.268(4) Å. The four Mn(1), N(11), Mn(1A), and N(11A) atoms also lie strictly on the same plane, but in contrast to **1**, the acute dihedral angle between the planes formed by two neighboring Mn_2N_2 units is 81.9(2)°, Figure 5. The torsion angle Mn(1)−N(21)···N(23)−Mn(1B) is 65.3(8)°. As occurs in **1**, the pyridyl rings bonded to the Mn(1) and Mn(1A) are roughly parallel (3.9° between them, separated by less than 4 Å), but in this case the high torsion angle between neighboring Mn_2N_2 end-on rings permits the extension of the $\pi-\pi$ interactions along the plane (angle between pyridyl rings from different Mn_2N_2 units 10.1°, separated by 4.25 Å), Figures 2 and 5. In this case it is interesting point out that the extensive $\pi-\pi$ interactions found in **2** force the large angle between the equatorial planes of neighboring Mn_2N_2 rings and may be one of the driving forces that stabilizes this high-dimensional systems. As occurs in **1**, the distance between the acetyl groups of different planes is lower than 3.5 Å.

Magnetic Data. The $\chi_M T$ product in the range 300−2 K and the molar magnetic susceptibilities *vs T* in the 300−20 K range of $[Mn(4\text{-CNpy})_2(N_3)_2]_n$ (**1**) and $[Mn(3\text{-acpy})_2(N_3)_2]_n$ (**2**) are plotted in Figure 6. As expected from the structural data, the two compounds show similar behavior: The $\chi_M T$ plots show a regular decay (room T $\chi_M T$ value is 3.70 $cm^3 \cdot K \cdot mol^{-1}$ for **1**

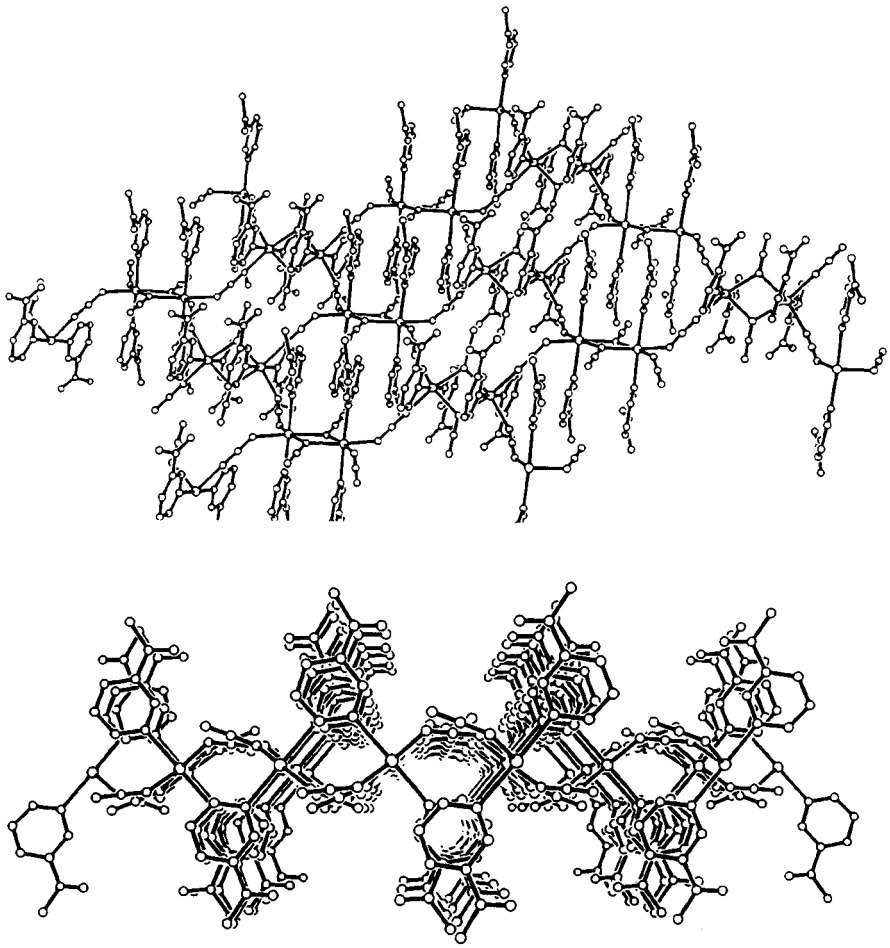

Figure 5. View of a sheet of $[Mn(3\text{-acpy})_2(N_3)_2]_n$ (**2**) showing the quasiperpendicular arrangement of the neighboring $Mn_2(1,1\text{-}\mu\text{-}N_3)_2$ units and perspective view of a sheet showing the differences with **1** in the arrangement of the *trans* 3-acpy ligands. In this case the pyridyl groups are placed roughly perpendicular, thus reducing the intersheet distance.

and 3.80 $cm^3 \cdot K \cdot mol^{-1}$ for **2**), down to 18 and 16 K critical temperatures, reflecting an overall antiferromagnetic behavior. Below T_C the $\chi_M T$ values abruptly reach the maximum value of 3.64 $cm^3 \cdot K \cdot mol^{-1}$ at 16 K for **1** and 9.57 $cm^3 \cdot K \cdot mol^{-1}$ at 12 K for **2**. The χ_M value increases when the temperature decreases from 300 K up to a maximum of susceptibility found at 38 K for **1** (3.79×10^{-2} $cm^3 \cdot mol^{-1}$) and 28 K for **2** (5.47×10^{-2} $cm^3 \cdot mol^{-1}$) due to the dominant antiferromagnetic coupling. After the maximum, the susceptibility value slowly diminishes and below T_C reaches abruptly 0.355 and 1.143 $cm^3 \cdot mol^{-1}$ at 2 K, respectively.

Magnetization measurements performed between ± 5 T at 2.5 and 3 K, respectively, indicate practically normal behavior for **1**, but they clearly show a magnetic hysteresis cycle and spontaneous magnetization for compound **2**, coercive field 1200 G, Figure 7. EPR measurements at room temperature show a sharp isotropic signal centered at $g = 2.0$ for both compounds, which strongly increases the peak-to-peak line width at low temperature. The line widths at 298 K are 40 and 51 G, whereas at 4 K they are 936 (**1**) and 561 G (**2**), according the expected EPR properties of 2-D ordered compounds at low temperature, Figure 8.[19] Low-temperature single-crystal measurements were not possible since the single crystals were too small and the intensity of the signal decreases at low temperature according the increase in line width.

These magnetic data clearly indicate two well-defined magnetic patterns for these compounds, a paramagnetic phase in which conventional superexchange is responsible for the magnetic properties and an ordered, low-temperature phase with T_C close to 18−16 K. Evaluation of the superexchange coupling constants in the paramagnetic region is not possible for a manganese 2-D system with one J ferro- and one J' antiferromagnetic parameters, and only a qualitative approach may be performed. Structural data indicate two kinds of interaction: Half the azido bridges show end-to-end coordination and, according to the bibliographical data, they should give an antiferromagnetic interaction (J_{AF}), whereas the other half of the azido bridges show end-on coordination for which ferromagnetic coupling (J_{FM}) is expected. Compounds **1** and **2** should thus be classified as alternating 2-D ferro−antiferromagnetic systems. Antiferromagnetic interaction becomes evident from the maximum in the χ_M *vs* T plots, and a greater J_{AF} should also be assumed for compound **1** (maximum at 38 K) compared to that for compound **2** (maximum at 28 K). This result agrees with the analysis of the J_{AF} with the bond and torsion angles recently published.[8,20] Effectively, compound **1** shows lower Mn−N−N and Mn−N−N−N−Mn′ angles than those for **2** (129.4(3), 141.1(3), and 58.0(5)° *vs* 140.1(2), 149.4(4), and 65.3(8)°, respectively), which permits a more effective overlap of the d_{z^2} atomic orbitals with the nonbonding π MO of the azido bridge allowing great antiferromagnetic coupling. Ferromagnetic interaction is less evident but may be indirectly inferred assuming a $J_{FM} = 0$ cm^{-1}, in which case the 2-D system is reduced to magnetically isolated AF manganese end-to-end

(19) Bencini, A.; Gatteschi, D. *EPR of Exchange Coupled Systems*; Springer-Verlag: Berlin, 1990; and references therein.

(20) Escuer, A.; Vicente, R.; Ribas, J.; El Fallah, M. S.; Solans, X.; Font-Bardia, M. *Inorg. Chem.* **1994**, *33*, 1842.

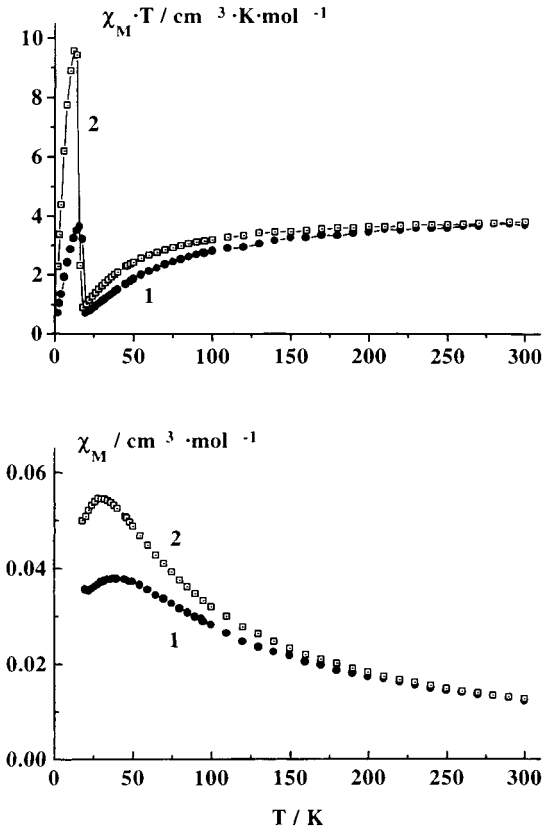

Figure 6. $\chi_M T$ *vs* T plots (top) in the 300−2 K range of temperatures and χ_M *vs* T plots (bottom) of the paramagnetic high-temperature region for $[Mn(4\text{-}CNpy)_2(N_3)_2]_n$ (**1**) and $[Mn(3\text{-}acpy)_2(N_3)_2]_n$ (**2**). The solid line in the $\chi_M T$ *vs* T plots is a guide for the eye.

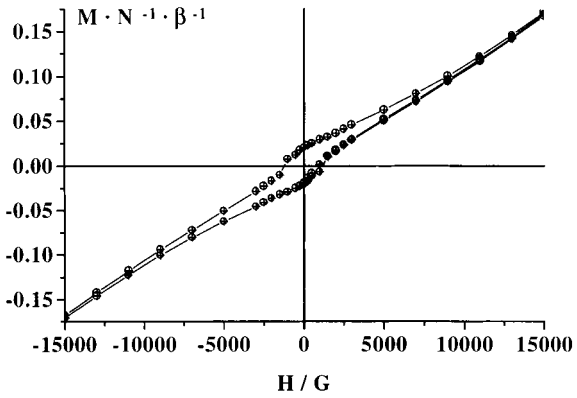

Figure 7. Hysteresis loop for $[Mn(3\text{-}acpy)_2(N_3)_2]_n$ (**2**). The solid line in the plots is a guide for the eye.

chains. Fitting the data under these conditions leads to unacceptably low χ_M plots which indicate a $J_{FM} > 0$ cm^{-1}. Therefore, more precise J values cannot be calculated.

The low-temperature properties such as the strong increase in the χ_M plots, the broadening of the EPR signals, and the spontaneous magnetization may be attributed to a canting phenomenon. Each $Mn_2(\mu_{1,1}\text{-}N_3)_2$ ferromagnetic unit is a high-spin center canted 20.9(1)° for **1** and 81.9(2)° for **2** with respect to the neighboring $Mn_2(\mu_{1,1}\text{-}N_3)_2$ units, in agreement with the more intense spontaneous magnetization and higher χ_M values reached for compound **2**.

The magnetic properties of the three previously reported compounds of this $[MnL_2(N_3)_2]_n$ series, in which L = pyridine (**3**), 4-acetylpyridine (**4**), and ethyl isonicotinate (**5**), were measured in a conventional susceptometer using a relatively high field of 1.5 T. In the light of the above results their magnetic properties were newly measured working under a low applied

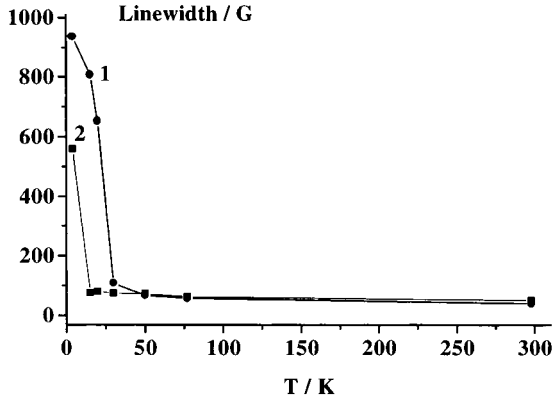

Figure 8. Plot of the variation of the EPR line width Δ_{pp} *vs* T for $[Mn(4\text{-}CNpy)_2(N_3)_2]_n$ (**1**) and $[Mn(3\text{-}acpy)_2(N_3)_2]_n$ (**2**).

Table 6. General Magnetic Properties for the Compounds of the $[MnL_2(N_3)_2]_n$ Series

	L				
	4-CNpy (**1**)	3-acpy (**2**)	py (**3**)	4-acpy (**4**)	Etinc (**5**)
T_C	18	16	40	28	16
$\chi_M T$(max)	3.63	9.42	2.26	9.71	3.77
intersheet d	13.579	11.268	(3-D)	11.563	15.760
α Mn planes	20.9	81.9	64.6	83.3	67.5
hys loop	No	Yes	No	Yes	Yes
Δ_{pp}(RT)[b]	40	51	26.3	32.2	45.3
Δ_{pp}(low T)	936 (4 K)	561 (4 K)	150 (33 K)	300 (30 K)	80 (4 K)

[a] The compund for which Δ_{pp} (4 K) is not reported corresponds to those where the EPR signal vanishes immediately after the 3-D ordering. [b] RT = room temperature.

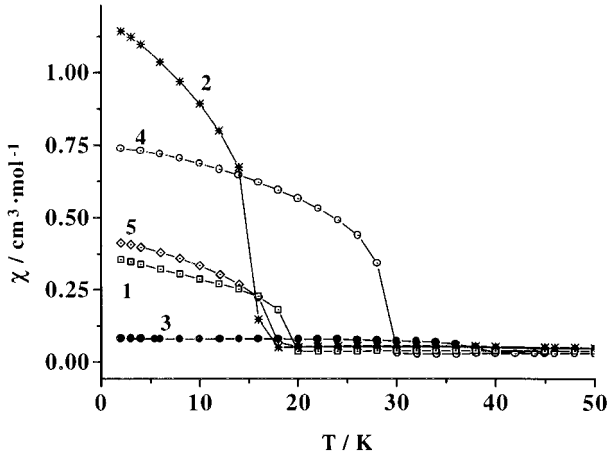

Figure 9. χ_M *vs* T plots of the low-temperature region for the **1**−**5** family of compounds $[Mn(L)_2(N_3)_2]_n$ showing similar behavior for all of them.

field of 100 G, and the results are similar to those reported for **1** and **2**: The three compounds are magnetically ordered as is shown in the data summarized in Table 6.

For this series of $[Mn(L)_2(N_3)_2]$ compounds T_C lies between 16 K for **2** or **5** and 40 K for **3**, Figure 9. Three of the compounds reported show spontaneous magnetization below T_C and remanent magnetization at zero field. It should be noted that spontaneous magnetization at low temperature was observed for antiferromagnetic compounds with only end-to-end azido bridges such as **4** and for end-to-end/end-on ferro−antiferro systems such as **2** or **5**. The common point between them is the high angle between the normal to the neighboring Mn−azido planes on the sheets. Intersheet interactions may also play a role in the value of T_c, but no evident relationship may be deduced from the limited structural data available.

On the other hand, it is expected that the T_C increases substantially by means of a stronger coupling.[21] Compounds **1**−**5** show low antiferromagnetic *J* superexchange constants, mainly due to the large Mn−N_1−N_2−N_3−Mn dihedral angle (defined as the angle between the Mn−N_1−N_2 and N_2−N_3−Mn planes), according to the study of the paramagnetic phase of the single azido bridge for nickel(II)[20] and manganese(II).[8] New related systems are currently being developed in order to increase T_C as function of the axial ligands.

(21) Néel, L., *Ann. Phys. (Paris)* **1948**, *3*, 137.

Acknowledgment. A.E. and R.V. thank the CICYT (Grant PB093/0772) for support of this research. F.A.M. thanks Prof. C. Kratky (University of Graz) for the use of experimental equipment.

Supporting Information Available: Listings of full data collection and processing parameters, bond lengths and bond angles, atomic coordinates, equivalent isotropic and anisotropic displacement coefficients, and hydrogen atom coordinates and isotropic displacement coefficients (13 pages). Ordering information is given on any current masthead page.

IC961476F